

Particle–wave association on a fluid interface

By SUZIE PROTIÈRE^{1,2}, AREZKI BOUDAUD²
AND YVES COUDER^{1,2}

¹Laboratoire Matière et Systèmes Complexes, UMR 7057 CNRS & Université Paris 7 – Denis Diderot,
ENS, 24 rue Lhomond, 75231 Paris Cedex 05, France

²Laboratoire de Physique Statistique de l'ENS, 24 rue Lhomond, 75231 Paris Cedex 05, France

(Received 15 July 2005 and in revised form 16 December 2005)

A small liquid drop can be kept bouncing on the surface of a bath of the same fluid for an unlimited time when this substrate oscillates vertically. With fluids of low viscosity the repeated collisions generate a surface wave at the bouncing frequency. The various dynamical regimes of the association of the drop with its wave are investigated first. The drop, usually a simple ‘bouncer’, undergoes a drift bifurcation when the forcing amplitude is increased. It thus becomes a ‘walker’ propagating at a constant velocity on the interface. This transition occurs just below the Faraday instability threshold, when the drop becomes a local emitter of a parametrically forced wave. A model of the particle–wave interaction accounts for this drift bifurcation. The self-organization of several identical bouncers is also investigated. At low forcing, bouncers form bound states or crystal-like aggregates. At larger forcing, the collisions between walkers reveal that their interaction can be either repulsive or attractive, depending on their distance apart. The attraction leads to the spontaneous formation of orbiting pairs, the possible orbit diameters forming a discrete set. A theoretical model of the non-local interaction resulting from the interference of the waves is given. The nature of the interaction is thus clarified and the various types of self-organization recovered.

1. Introduction

This article is devoted to the various regimes of interaction of localized structures formed by the association of drops bouncing on a fluid surface with the surface waves they excite. The stabilization of drops by bouncing was first observed on an oscillating soap solution (Walker 1978). It was shown recently (Couder *et al.* 2005a) to exist also in pure fluids and to be due to the dynamics of the air film. At each oscillation, as the drop hits the bath, an air film is squeezed between the two fluids. This film has no time to break before the drop lifts off again, when the downward acceleration of the bulk fluid becomes large. A steady regime is thus reached where the drop never has enough time to coalesce with the substrate. In our previous work (Couder *et al.* 2005) this phenomenon was investigated in very viscous fluids where the stabilization of drops of typical diameters 1 to 3 mm was observed at driving frequencies ranging from 30 to 200 Hz. With small drops in the low-frequency range, the peak acceleration had simply to be larger than gravity g . This is the condition of lift-off for an inelastic solid body placed on a vertically oscillated solid plate (Pieranski 1983; Tuffillaro & Albano 1986). With very viscous fluids, the collision of the drop does not excite surface waves but generates a simple trough in the interface. In between two bounces, this trough relaxes partially. In the present article we obtain the same phenomenon of

coalescence in fluids with small viscosities (in the range $5 \times 10^{-3} < \mu_L < 0.1$ Pa s). The viscous length scale is now much smaller than the wavelength of the surface wave at the driving frequency so that the bouncing can excite these waves on the surface (figure 1). Our results concern the dynamics, the interactions and the self-organization of these particle–wave associations.

We will show that they are related to the behaviours of the two-dimensional nonlinear localized states (LS). We briefly recall some of the results concerning the existence of the LSs, their interactions and self-organization. In spatially extended homogeneous systems, instabilities usually lead to the formation of uniformly distributed patterns, limited only by the system’s boundaries. However, localized structures can also be generated that are associated with sub-critical bifurcations (Fauve & Thual 1990; Deissler & Brand 1991). These LS can exist when the value of the control parameter is in the hysteretic region and when small domains undergo a transition to the bifurcated state, the rest of the field remaining in the basic state. These so-called ‘local states’ (LS), the equivalent of solitons in dissipative systems, are stable in two dimensions. It is of particular interest here that such structures were observed in sub-critical variants of the Faraday instability. Called ‘oscillons’ in vibrated sand (Umbanhowar, Melo & Swinney 1996) they also exist in very thin layers of viscous fluids (Lioubashevski, Arbell & Fineberg 1996). More generally, a vast literature has been devoted to the interactions of localized states in model equations (e.g. Aranson *et al.* 1990; Moskalenko, Liehr & Purwins 2003), in the context of nonlinear optics (Schäpers *et al.* 2000; Desyatnikov & Kishvar 2002; Vladimirov *et al.* 2002) or in reaction diffusion systems (Schenk *et al.* 1998; Liehr *et al.* 2004), showing that they have particle-like interactions leading to their static aggregation or to orbital motion.

In the present work, using bouncing drops slightly below the threshold of the Faraday instability, we obtain point-like mobile sources of Faraday waves. We thus excite localized waves in the vicinity of a super-critical bifurcation. The resulting objects, which associate a particle and a wave, have non-local interactions. Their self-organization leads to the formation of a great variety of bound or orbiting states. Preliminary results on this experiment were published in Couder *et al.* (2005*b*) and Protière *et al.* (2005).

2. Experimental set-up

A square container ($8 \times 8 \times 1$ cm) is partly filled with a layer of silicon oil of thickness $h = 4$ mm. It is placed on a vibration exciter (Bruel and Kjaer 4809) driven by the sinusoidal signal of a low-frequency generator. The resulting motion gives the fluid a vertical acceleration $\gamma = \gamma_m \cos(2\pi f_0 t)$ where the frequency is in the range $15 < f_0 < 300$ Hz and the amplitude can take values from 0 to 20 g.

The container was carefully manufactured and set horizontally and perpendicular to the vibration axis. The fine-tuning was done by approaching the Faraday instability and checking that the waves emitted by the four bordering menisci were of identical amplitudes.

The chosen fluids were silicon oils because their surface is not sensitive to surfactant effects. We explored a range of viscosities from $\mu_L = 5 \times 10^{-3}$ Pa s to 0.1 Pa s. Most of the results reported here were obtained with Rhodorsyl oil 47 V 20 and 47 V 50 which have viscosities $\mu_L = 20 \times 10^{-3}$ and 50×10^{-3} Pa s, respectively, surface tension $\sigma = 0.0209$ N m $^{-1}$ and density $\rho = 0.965 \times 10^3$ kg m $^{-3}$. The amplitude of the imposed oscillation was below the threshold for the Faraday instability so that the upper

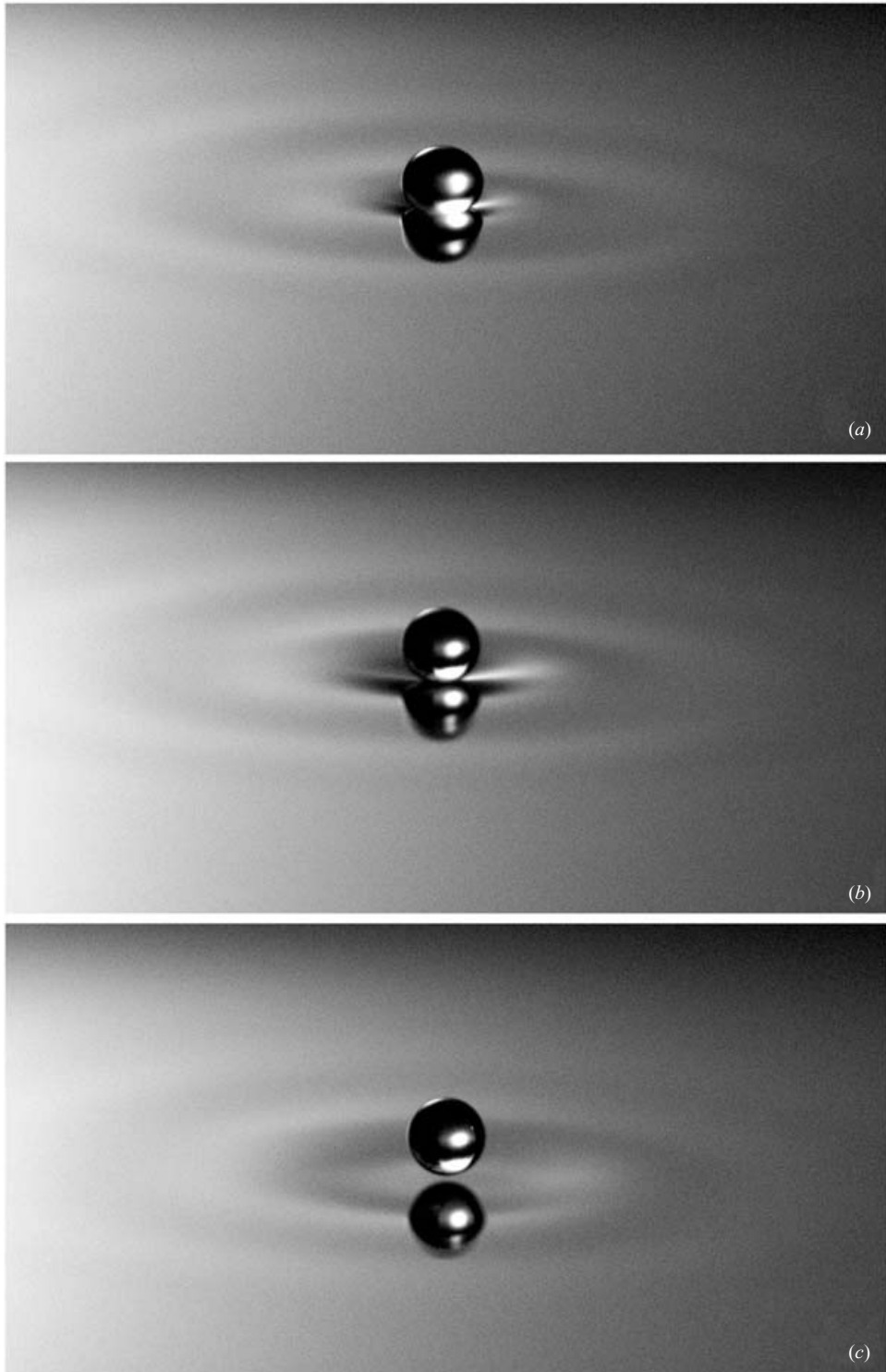


FIGURE 1. Three photographs showing a drop as it bounces on the surface of a bath of the same fluid oscillating vertically. Note the resulting travelling wave emitted on the liquid surface at the forcing frequency. ($D = 1$ mm, $\mu_L = 20 \times 10^{-3}$ Pa s, $f_0 = 80$ Hz, $\gamma_m/g = 3$). The photographs correspond to half a period of the forcing ($T_0/2 = 6$ ms).

surface of the bath was stable. An accelerometer was used to measure the acceleration γ imposed by the forcing.

With fluids of weak viscosity, it is difficult to sustain drops with $D > 1.5$ mm as the flow of the air film sets the oil into motion so that the film drains faster. Smaller drops $0.1 < D < 1.5$ mm are seen to bounce on the surface very easily. In order to create such small drops on a viscous oil, we dip a pin into the vibrating bath, then remove it swiftly. The breaking of the liquid bridge between the pin and the bath generates drops with $0.1 < D < 1$ mm. Repeating the process, we obtain a number of drops of various sizes, simultaneously bouncing on the surface. We observe these drops with a strong magnification and only retain those we need, usually chosen of identical sizes. The others are then carefully removed by picking them up with the needle. The lifetime of the drops being very long, they can be used for experiments lasting several hours. It is possible to displace a drop at will by poking the interface with a needle. The meniscus surrounding the needle acts as a repeller; thus, by approaching it, the bouncing drop can be pushed gently without the drop itself being touched.

The motion of the drops can be decomposed into two components having different time scales. There is a rapid bouncing motion as well as a slower mean horizontal propagation. The former can be recorded with a fast video camera ($1000 \text{ images s}^{-1}$). Observing it from the side we used an image processing system to single out the evolution with time of one vertical line of the image. This provides recordings of the vertical trajectory of the drop and of its reflection on the bath. A stroboscope and a classical videotape recorder are better adapted to observing the slower horizontal propagation of the drops. The surface is illuminated from the top with a diffuse light having an intensity gradient. A semi-transparent mirror set at 45° angle is placed in between the light source and the fluid bath. The reflection of the fluid surface in this mirror is filmed, providing non-distorted images of the surface as observed from the top.

3. The various regimes of bouncing of a single drop

Figure 1 shows the bouncing of a drop deposited on the oscillating bath. This phenomenon depends on at least five parameters: μ_G the viscosity of the gas, μ_L the viscosity of the liquid, D the drop diameter, f_0 the forcing frequency and γ_m the amplitude of the oscillating acceleration. Its complete exploration is beyond the scope of the present article. For the viscosity and frequency dependence we can only present trends. The bouncing of drops was obtained in silicon oil in a large viscosity range $5 \times 10^{-3} < \mu_L < 0.1$ Pa s. The typical diameters of drops that can be sustained decrease for fluids of small viscosity. Correspondingly the frequencies efficient in generating bouncing are shifted towards larger values (Couder *et al.* 2005a).

Most experiments reported here were done using two oils of small viscosity ($\mu_L = 20 \times 10^{-3}$ and 50×10^{-3} Pa s) at fixed forcing frequencies. As μ_L and f_0 are fixed, we can draw a phase diagram showing the different dynamical behaviours observed as a function of the drop diameter D and γ_m/g , the ratio of the acceleration amplitude to gravity. The diagram in figure 2 was obtained with $\mu_L = 50 \times 10^{-3}$ Pa s at $f_0 = 50$ Hz. A very similar diagram with only slightly shifted limits was obtained with $\mu_L = 20 \times 10^{-3}$ Pa s at $f_0 = 80$ Hz. In these diagrams, two thresholds set the limit of the region of interest.

The lowest limit is the minimum acceleration γ_m^B/g needed to sustain bouncing. Below this threshold the drops coalesce with the substrate in a few tenths of a second. The other limit is the Faraday instability. The threshold acceleration

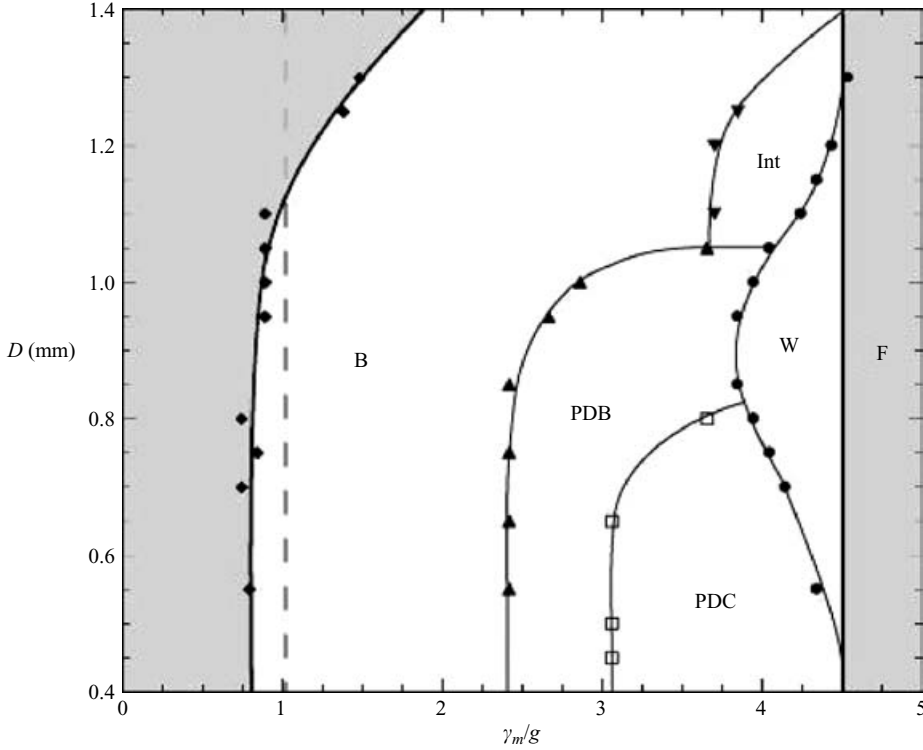


FIGURE 2. Phase diagram of the various behaviours of a drop as a function of its diameter D and of the forcing acceleration γ_m/g , for a silicon oil with $\mu_L = 50 \times 10^{-3}$ Pa s oscillated at frequency 50 Hz. The behaviours in the various domains are the following. In B there is simple bouncing, in PDB period-doubling, in PDC transition to temporal chaos by a period-doubling cascade, in Int the drop has an intermittent behaviour, W is the region of walkers and F the Faraday instability domain.

γ_m^F of this instability was investigated as a function of the viscosity and the forcing frequency, in low-viscosity fluids and assuming infinite depth, with the result $\gamma_m^F = 2^{4/3}(\rho/\sigma)^{1/3}\mu_L(2\pi f_0)^{5/3}$ (Edwards & Fauve 1994 and Fauve private communication). Working with various oils we recover this result. In the case of figure 2 where $\mu_L = 50 \times 10^{-3}$ Pa s and $f_0 = 50$ Hz, we find $\gamma_m^F/g = 4.5$. Above this threshold, standing waves appear on the whole surface of the liquid due to the parametric forcing. The drops still bounce on the wavy surface but their motion is very chaotic and this generates irregular collisions and ultimately coalescence.

3.1. Simple bouncing

In the region B of figure 2, the drops bounce on the substrate at the forcing frequency (figure 3*a*). For drops with $0.2 < D < 1.2$ mm (at $\mu_L = 50 \times 10^{-3}$ Pa s) the threshold for bouncing γ_m^B/g is close to 1. Dynamically, the non-dimensional number which characterizes the deformation of a drop during the collisions is the Weber number $We = \rho V^2 R / \sigma$, the ratio of the kinetic energy of the drop to its surface energy. Here the Weber number is small so that the drop remains approximately spherical. Hence the condition for bouncing is close to that for an inelastic solid mass to lift off from a vertically oscillating substrate: $\gamma_m^B = g$. As seen on figure 2, for very small drops, the threshold is $\gamma_m^B/g < 1$. This means that some elastic energy, due to surface tension,

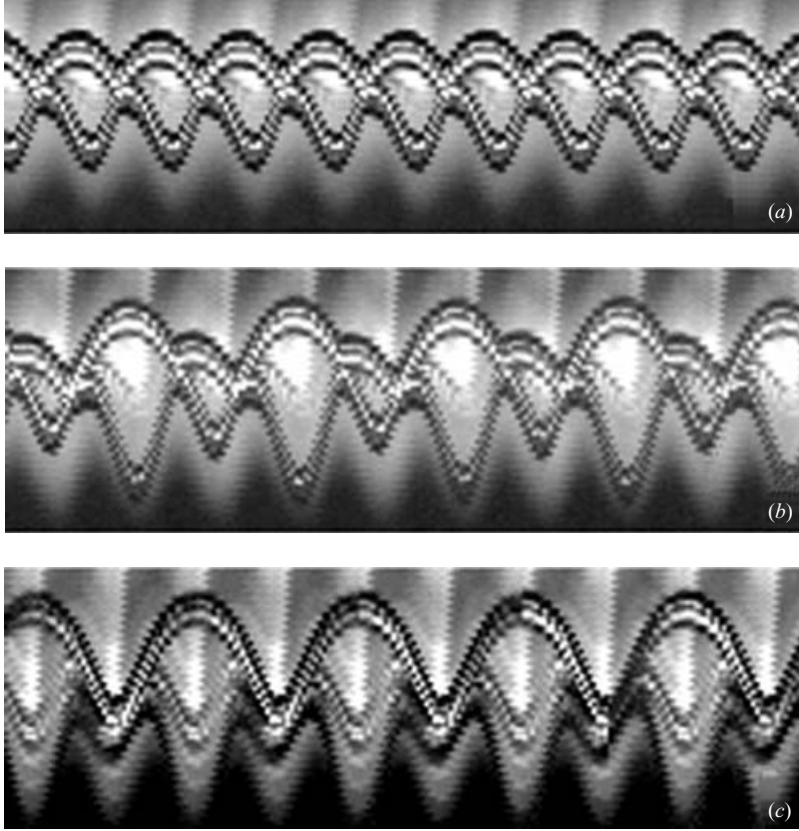


FIGURE 3. Three spatio-temporal diagrams $z(t)$ showing the vertical trajectory of a small drop and of its reflection on the oscillating surface. Time elapses from left to right. (a) The simple bouncing regime with $\gamma_m/g = 2.5$. The amplitude of the droplet jump (~ 0.13 mm) is of the same order of magnitude as the amplitude of the surface oscillation ($A_b \sim 0.10$ mm). (b) Period doubling at $\gamma_m/g = 3.5$. (c) The walker regime at $\gamma_m/g = 4.3$, ($D = 1$ mm, $\mu_L = 20 \times 10^{-3}$ Pa s, $f_0 = 80$ Hz). The amplitude of the droplet jump (~ 0.30 mm) is now much larger than the amplitude of the surface oscillation ($A_F \sim 0.16$ mm).

is stored in the drop so that the restitution coefficient is non-zero. At the other extreme, for large drops ($D > 1$ mm), the threshold for bouncing γ_m^B/g becomes larger than 1. Such super-inelastic collisions have been previously investigated (Couder *et al.* 2005a). They occur in situations where the film separating the drop from the substrate becomes wide and thin during the collision. Extra energy is needed to suppress the resulting adhesion and this effect accounts for the increase of the threshold.

3.2. Period-doubled bouncing

When the control parameter γ_m/g is increased, the evolution of the drop's vertical motion depends on its size.

(i) Large drops ($D > 1.2$ mm) simply keep bouncing at the forcing frequency in a large range of values of γ_m/g . Ultimately, their vertical motion shows intermittent disorder (region Int of figure 2) which will not be investigated here.

(ii) For small drops the successive jumps become alternately large and small (figure 3b) so that the period doubles (region PDB of figure 2). When $D < 0.6$ mm, this process repeats itself in a period doubling cascade (PDC on figure 2) leading to a

temporally chaotic motion. This is exactly the behaviour of a solid ball on a vertically oscillating solid substrate (Pieranski 1983; Tuffillaro & Albano 1986).

(iii) The most interesting phenomenon occurs for drops of intermediate size, $0.8 < D < 1.1$ mm. In this range, the motion undergoes only one period doubling before entering region W (figure 2) where the drop starts moving at a constant velocity in the horizontal plane. For simplicity we will call these bouncing and drifting drops ‘walkers’. Using oils of various viscosities forced at other frequencies, we find that the domain of existence of these walkers is always located just below the Faraday instability threshold and is directly linked to it.

(iv) Smaller $0.6 < D < 0.8$ mm and larger $1.1 < D < 1.2$ mm drops also reach a walking regime by synchronization but after a somewhat more complex evolution.

3.3. A drift bifurcation: the walkers

Observation with the fast camera reveals that the limit of region W corresponds to the values of γ_m/g at which the period doubling becomes complete. The drop thus touches the surface only once in two driving periods (figure 3c). Correspondingly the drop spontaneously acquires a horizontal translation motion on the surface of the bath with a well-defined velocity V_w . This velocity depends on the size of the drop (the larger drops being faster) and increases with γ_m . This motion is intrinsic and results from the interaction of the drop with the wave it generates (figures 4 and 5). The velocity of the drop which is in the range $0 < V_w < 20$ mm s⁻¹ remains small compared to the velocity V_F^φ of the surface waves forced by the drop at the Faraday frequency ($V_F^\varphi = 189$ mm s⁻¹ for a Faraday frequency $f_F = f_0/2 = 40$ Hz).

We investigated the transition from bouncing to walking and figure 7(a) shows the evolution of the non-dimensional velocity V_w/V_F^φ of three drops when the control parameter γ_m/g is increased. For the two smaller drops ($D = 0.56$ and 0.7 mm) the transition is super-critical at a well-defined threshold. The velocity of the walker grows as the square root of the distance to the threshold. For the larger drops ($D = 0.86$ mm), the bifurcation is sub-critical with a large hysteresis. This transition is a drift (or parity breaking) bifurcation similar to those first observed in one-dimensional extended patterns (as in e.g. Rabaud, Michalland & Couder 1990) and modelled in Ginzburg–Landau models (Coulet, Goldstein & Gunaratne 1989). They were also theoretically investigated in the case of localized states (Osipov 1996). The spontaneous motion of large-amplitude, localized waves packets was observed in Faraday experiments performed on thin fluid layers driven at very high forcing amplitudes by Lioubashevski *et al.* (1996).

The particle–wave interaction

The mechanism by which this transition from bouncing to walking occurs is linked with the interaction of the particle with the wave and can be directly observed.

The region W lies below the Faraday threshold γ_m^F . The interface is thus stable everywhere (except in the vicinity of the cell’s borders where weak waves are generated by the bordering menisci). The drop itself, bouncing at $f_0/2$, emits travelling waves. Their measured wavelength λ_F is in excellent agreement with the wavelength obtained by setting $\omega_F = 2\pi(f_0/2)$ in the dispersion relation:

$$\omega^2 = \{gk + (\sigma/\rho)k^3\} \tanh(kh). \quad (1)$$

These waves are thus the travelling equivalent of the Faraday standing waves usually observed.

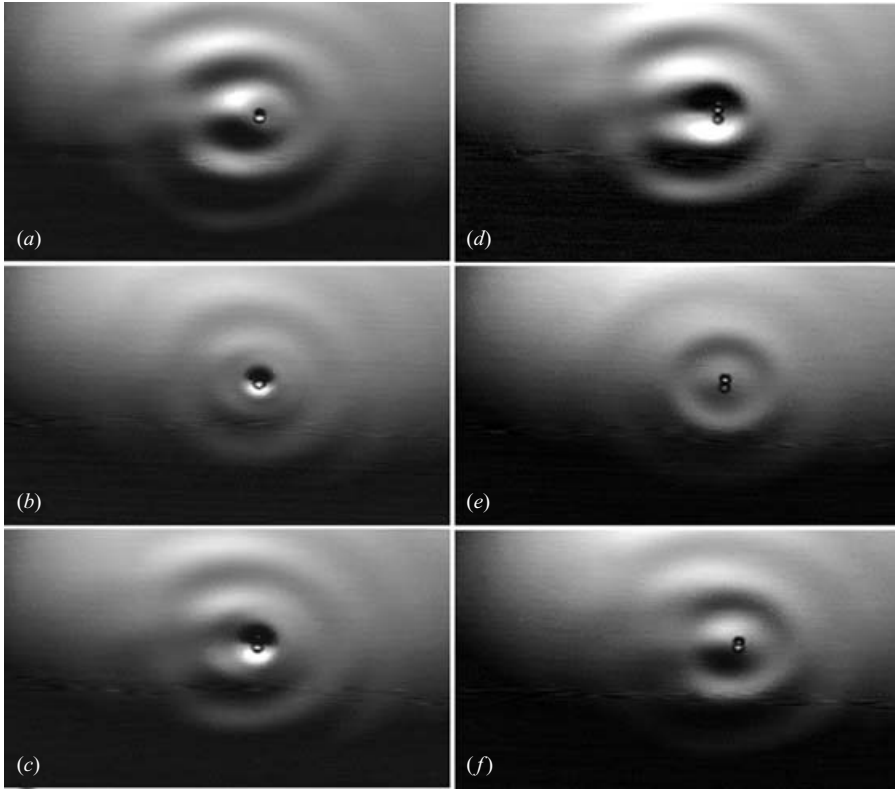


FIGURE 4. Six photographs showing the motion of a walker and of the travelling wave it emits on the liquid surface as seen from the top. The photographs cover two forcing periods. Photographs (a) and (b) are taken when the drop comes into contact with the liquid interface. ($D = 0.65$ mm, $\mu_L = 20 \times 10^{-3}$ Pa s, $f_0 = 80$ Hz, $\gamma_m/g = 3.5$).

Observation with the fast camera shows that the drop's motion is composed of a series of identical parabolic jumps (figure 5). This motion is sustained by a lock-in phenomenon with the wave. The drop is in contact with the bath through an air film for approximately a fifth of the Faraday period. When the drop hits the bath, the collision forms a small crater in the surface (figures 4–6). The drop then lifts up and the wave created by the shock evolves freely, the edge of the crater forming the crest of a circular wave propagating radially. As time elapses the surface at the centre of this crater bulges to form a spherical cap protrusion. This protrusion will have maximum amplitude one forcing period later. The drop hits the surface again a little later when this protrusion is spreading with decreasing amplitude. The impact with the surface occurs on the side of the protrusion, on an inclined surface. During this collision, the vertical component of the drop's velocity is reversed, while the horizontal one is sustained. Its free trajectory will again be an arc of a parabola. In the steady regime this motion will, one Faraday period later, cause the drop to collide with the surface at the same position on the 'forward side' of the next protrusion (figures 4, 5 and 6).

The relation between the drop and the wave is sketched on figure 6. Each time the drop hits the surface a new dip forms, shifted from the trough that would have been formed by the evolution of the previous wave-packet. The resulting wave is thus the

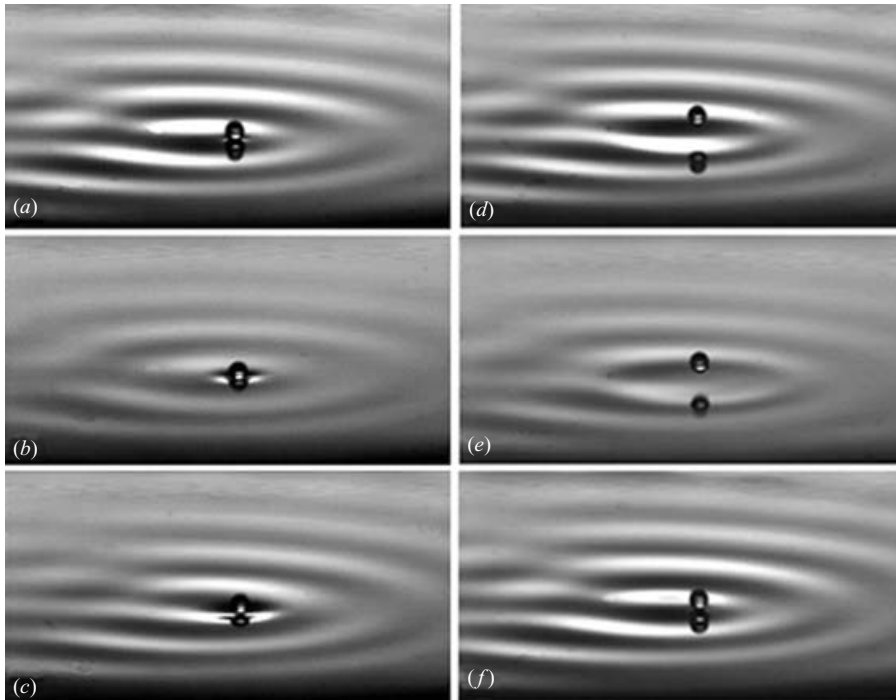


FIGURE 5. Six photographs showing the motion of a walker and the travelling wave it emits on the liquid surface as seen from the side. The photographs cover two forcing periods. ($D = 0.75$ mm, $\mu_L = 20 \times 10^{-3}$ Pa s, $f_0 = 80$ Hz, $\gamma_m/g = 3.5$).

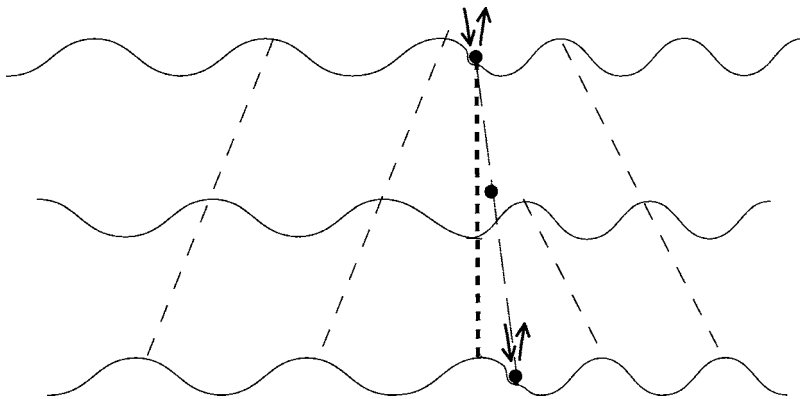


FIGURE 6. Sketch of the motion of a walker and of its interaction with the wave it emits. Note the Doppler shifts of the waves emitted forwards and backwards. For simplicity the droplet velocity is shown larger than actually observed. The waves are drawn of constant amplitude, which is not realistic: in reality the amplitude is strongly modulated in time by the forcing (see figure 5). They also decay with the distance to the source.

superposition of waves generated by a source that is slightly displaced at each jump. For very fast walkers this creates a Doppler effect and the wavelength is reduced ahead of the moving drop and increased behind. Owing to these frequency shifts, the parametric forcing becomes less effective and the waves emitted forwards and backwards by a walker have weaker amplitudes than those emitted laterally (figure 4).

Near the Faraday threshold, a walker mostly generates two symmetrical lateral waves. When the threshold is reached, the waves generated by the drop cover the whole cell. As they reach the boundaries the standing waves form the pattern of the classical Faraday instability.

3.4. A model for the particle–wave interaction

The interaction of the drop with the surface can be represented by the following equation for the drop's horizontal motion, which is averaged over a period of the sub-harmonic vertical motion and assumed to take place in the direction of the x -axis:

$$m \frac{d^2x}{dt^2} = F^b \sin\left(2\pi \frac{dx/dt}{V_F^\varphi}\right) - f^v dx/dt. \quad (2)$$

The left-hand side stands for the inertia of the drop, $m \sim 1$ mg being its mass. On the right-hand side are the forces exerted during the collision (which lasts a time τ), averaged over one Faraday period T_F . Here, as seen above $\tau/T_F \sim 0.2$. The first term is the effective force due to the bouncing on an inclined surface; $F^b \sim m\gamma_m(A_F/\lambda_F)(\tau/T_F) \sim 10^{-6}$ N is proportional to the amplitude of the vertical acceleration γ_m and to the slope of the generated surface waves. This slope is approximately A_F/λ_F where $A_F \sim 0.5$ mm is the amplitude and λ_F the wavelength of the surface wave at the Faraday frequency ($\lambda_F \sim 5$ mm for $f_F = 40$ Hz). The tilt of the surface (figure 6) at the time of collision results from the difference in propagation of the drop (moving with velocity $V_W = dx/dt$) and the wave (of phase velocity V_F^φ) since the previous collision. The argument of the sine corresponds to this phase shift. The last term stands for the viscous damping due to the shearing of the air layer between the drop and the bath during the contact; $f^v \sim (\mu_G s/h_f)(\tau/T_F) \sim 10^{-6}$ N m $^{-1}$ s is the effective damping based on the viscosity of air μ_G , the ‘area of contact’ between the drop and the bath $s \sim 1$ mm 2 and the typical thickness of the film $h_f \sim 2$ μ m.

Seeking steady regimes of the system, and in the limit of small velocities, equation (2) gives,

$$\frac{V_W}{V_F^\varphi} \left[2\pi F^b - \frac{8\pi^3}{6} \left(\frac{V_W}{V_F^\varphi} \right)^2 F^b - f^v V_F^\varphi \right] = 0. \quad (3)$$

For small values of F^b only the motionless solution $V_w = 0$ is possible. But it becomes unstable when F^b becomes larger than a bifurcation threshold F_c^b :

$$F_c^b = f^v (V_F^\varphi/2\pi). \quad (4)$$

Above this threshold, two stable solutions with $V_w \neq 0$ appear with

$$V_w/V_F^\varphi = \pm(\sqrt{6}/2\pi) \sqrt{(F^b - F_c^b)/F^b} \quad (5)$$

and a transition from no translation to walking occurs. The drop can move either to the right or to the left at constant velocity (or in any direction if the equation was written in two dimensions). This system, where the control parameter is F^b , undergoes a supercritical pitchfork bifurcation. The order parameter (the non-dimensional velocity V_w/V_F^φ) varies as the square root of the distance to threshold. This bifurcation is similar to a drift bifurcation, although its origin is different. Figure 7(b) shows the bifurcation as computed from equation (3). We can see that in this simulation there is only one parameter, so that the bifurcation is the same for all drops. Experimentally the bifurcation threshold as well as its type (super- or sub-critical) depends on the drop size. The existence of a hysteresis for a large drop might

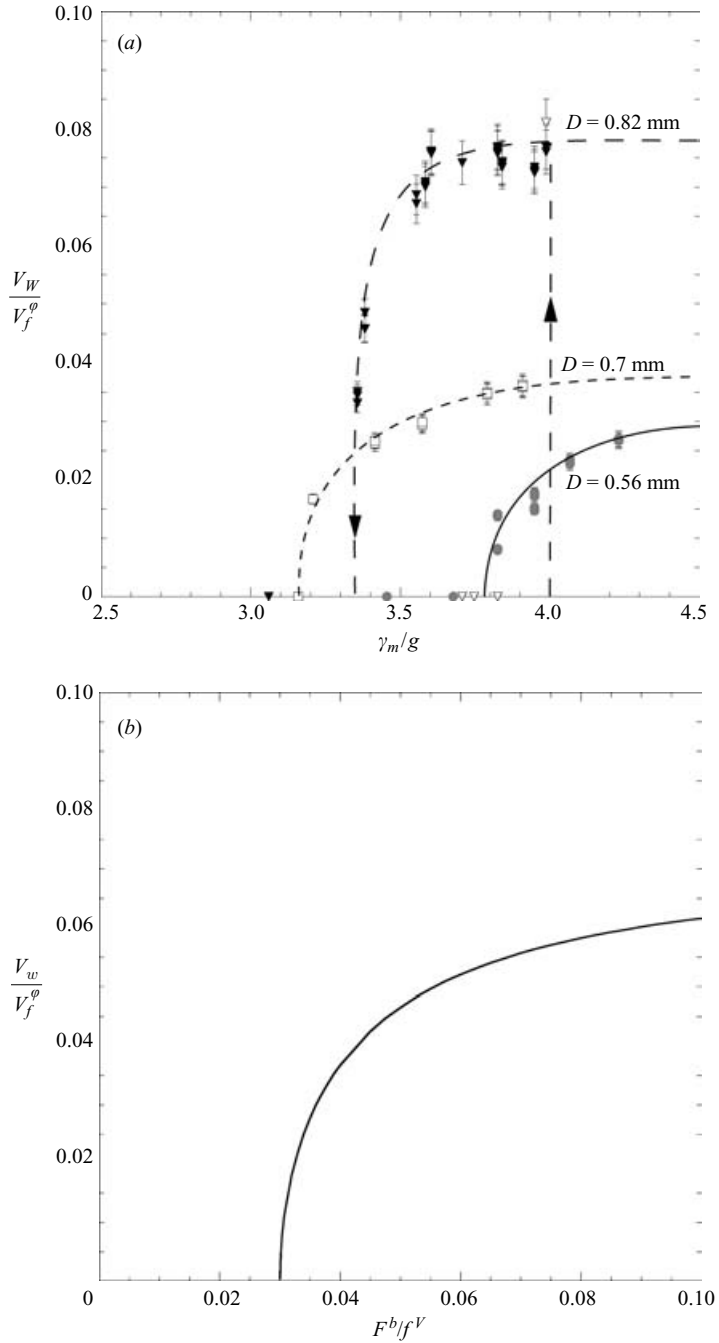


FIGURE 7. (a) The non-dimensional horizontal velocity V_W/V_f^ϕ of three walkers of different diameters as a function of the forcing acceleration γ_m/g ($\mu_L = 20 \times 10^{-3}$ Pa s, $f_0 = 80$ Hz). The arrows show the hysteric cycle observed for the largest drop $D = 0.87$ mm for which the transition to walking is sub-critical. (b) The horizontal velocity of a walker obtained in the model (equation (3)) as a function of the model's control parameter F_b/f^V .

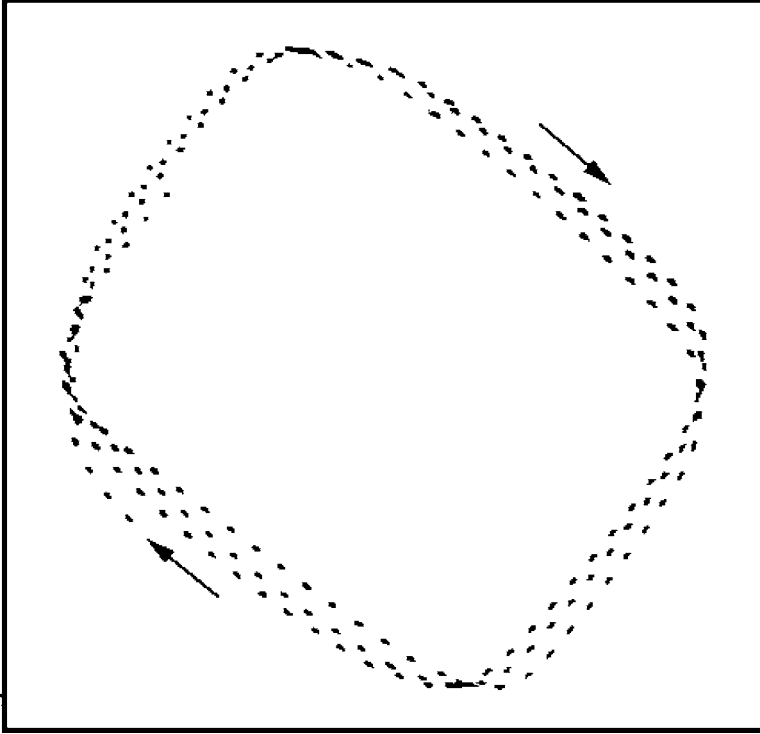


FIGURE 8. The stroboscoped walker's trajectory during three periods of a billiard-like motion in a square cell ($8\text{ cm} \times 8\text{ cm}$). This trajectory was obtained by the superposition of images where only the drop was lit. The black frame corresponds to the walls of the cell. The minimum distance of approach of the drop to the wall is $\sim \lambda_F$. The angle of incidence (relative to the normal to the wall) is $i = 38^\circ$ while the angle of reflection is $i' = 53^\circ$ ($\mu_L = 50 \times 10^{-3}\text{ Pa s}$, $f_0 = 50\text{ Hz}$, $\gamma_m/g = 4$, $V_w = 18\text{ mm s}^{-1}$).

be due to the longer contact time or to the effect of the deformation of the drop during its collision with the bath, neither of which is taken into account in the model.

3.5. The billiard motion

When a walker approaches one of the boundaries of the cell, it is repelled and undergoes a reflection without touching the wall. In a square cell, as shown on figure 8, the drop is thus observed to have a motion similar to an undamped classical billiard ball, but with the following specific features. The first one is that during the collisions the drop remains at a finite distance from the boundary and has a curved trajectory with no singularity. This is linked to the spatial extent of the wave. The closest approach to the walls on figure 8 is of the order of the wavelength λ_F . A second characteristic is that the angle of incidence and the angle of reflection are not equal. The reflection results from the interaction of the drop with a wave formed by the superposition of the drop's wave, its reflection in the boundary, and the wave emitted by the boundary meniscus. The complete investigation of this effect is beyond the scope of the present article. Far from the Faraday threshold the damping length of this wave is small, so that the drop turns back close to the wall. For values of γ_m/g closer to the Faraday threshold, the wave extent becomes large and the collision corresponds to an increasingly non-local interaction, the drop always remaining far from the boundary.

4. The interaction and self-organization of several drops

A remarkable feature of bouncing drops is that they are mobile sources of surface waves. Their motion results from the interaction of the drops with the sum of the waves they generate. These waves have a frequency fixed by the bouncing. Their length of damping depends on the fluid viscosity and on the value of D and γ_m/g .

Three types of situations are observed corresponding to the excitation by a drop of different waves:

- (i) When the waves are strongly damped, compact aggregates form.
- (ii) When surface waves are generated at either the forcing frequency or half of it, bound states are formed where the drops stabilize at well-determined distances from each other. When many identical drops are present, two-dimensional crystalline arrangements form.
- (iii) The walkers, interacting through the interference of the surface waves they emit at the Faraday frequency, have dynamical behaviours such as various orbital motions or chaotic trajectories.

4.1. Self-organization of simple bouncers

Aggregation into dense clusters

In the very viscous fluid ($\mu_L > 10^{-1}$ Pa s) investigated previously (Couder *et al.* 2005a), each drop, as it collides with the surface, deforms it into a small depression. This is also observed in the present set of experiments for $\mu_L = 50 \times 10^{-3}$ Pa s when large drops $D > 1.2$ mm are just above their bouncing threshold. In these cases, when two drops are simultaneously present in the cell, there is a weak attractive interaction between the troughs they generate. The drops, following adiabatically the drift of their troughs, are observed to move slowly towards each other. This attractive interaction between drops is analogous to the interaction between small floating objects due to the menisci they create (Chan, Henry & White 1981). When the drops ultimately come into near contact, they usually remain separated by a stable air film. If several identical drops are deposited on the surface they ‘condense’ to form stable rafts with a dense triangular lattice (figure 9a).

Bound states and crystalline patterns

Remaining in region B of the phase diagram, when γ_m/g is increased, the self-assembly changes. Two identical bouncers will still drift towards each other but they now stop at a finite distance d_0^{bd} apart, where they remain bound. If two drops had previously condensed next to each other, they will repel when γ_m/g is increased and stabilize at d_0^{bd} apart. In this regime the non-local interaction between drops is due to the damped surface wave each of them emits. In the self-organized stable arrangement each drop is at such a position that its successive collisions with the interface leave it motionless. Each drop, in region B, oscillates at the forcing frequency and the wave it emits is strongly damped. In this region only one value of d_0^{bd} is observed; it is slightly smaller than λ_0 , the wavelength of the surface wave at the forcing frequency.

When three drops bind to each other, they form an equilateral triangle of side d_0^{bd} . This is the building block of the self-assembly of larger crystal-like structures which are observed when more drops keep aggregating. Figure 9(b) shows a two-dimensional crystallite formed by seven identical drops.

These bound states and clusters are very similar to those predicted theoretically for the self-organization of localized states (Aranson *et al.* 1990; Vladimirov *et al.* 2002). Such clusters were observed experimentally in sub-critical Faraday experiments (in sand, Umbanhowar *et al.* 1996, or in thin fluid layers, Lioubashevski *et al.* 1996),

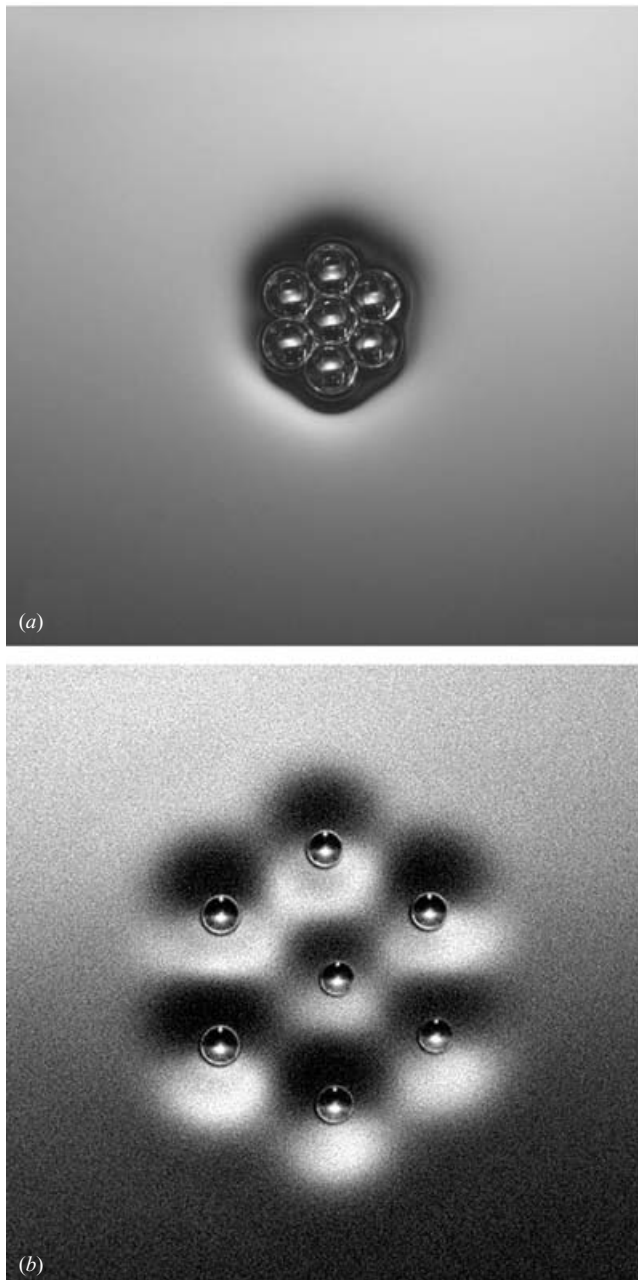


FIGURE 9. (a) A compact aggregate of seven large drops in a viscous oil ($\mu_L = 500 \times 10^{-3}$ Pa s, $f_0 = 30$ Hz, drops diameter $D = 2$ mm). (b) An example of the self-assembly of seven steady bouncers into a cluster with a crystalline triangular lattice. The photograph is taken when the deformation of the surface is maximum ($\mu_L = 20 \times 10^{-3}$ Pa s, $f_0 = 56$ Hz, $D = 0.66$ mm, $d_0^{bd} = 2.5$ mm).

in reaction diffusion systems (Schenk *et al.* 1998) and in nonlinear optics (Schäpers *et al.* 2000; Desyatnikov & Kishvar 2002).

When the drops forming the aggregate are of different sizes, the emitted wave is not of the same amplitude in every direction, being weaker on the side with small drops.

The reaction will thus generate a spontaneous displacement of the whole aggregate on the surface. The simplest case is that of two drops which will move slowly as a pair, the small drop leading the way.

In the PDB region the same types of bound states and crystalline aggregates are observed but the successive jumps are now uneven. The bouncing drops excite a superposition of waves of frequency f_0 and $f_0/2$, the latter becoming dominant when γ_m/g is increased. Two particles forming a bound state a distance d_0^{bd} apart are thus observed to move away from each other and stabilize at a new distance d_1^{bd} which is usually slightly smaller than the wavelength λ_F , the Faraday wavelength associated with frequency $f_0/2$. Other bound states at distances apart of d_2^{bd} slightly smaller than $2\lambda_F$ are observed. However these are not the only possible states. Because of the period doubling, the drops can have two different phases relative to the forcing. In the case where the larger jumps of the two drops occurs at opposite phases, the observed distances d_n^{bd} follow $(n + 1/2)\lambda_F$, the closest pair corresponding to $n = 0$. This will be discussed in more detail for walkers.

4.2. The interactions and dynamical behaviour of several walkers

Scattering of two identical drops

Let us now consider the situation where two walkers (that we will choose identical) are present in the same cell. Both of them will have a billiard motion so that, inevitably, they will come close to each other. During these encounters the trajectories of the drops are deflected even though the drops themselves do not touch each other. A variety of events can be observed.

For some values of the collision parameters the walkers repel each other as shown on figure 10(a). In the simplest cases the drops have roughly hyperbolic trajectories and the modulus of their velocities is unchanged after the collision. For collisions with different initial conditions an attraction is observed between the walkers, which can lead to a capture where the drops start orbiting around each other (figure 10b).

In some instances, both in the repulsive and attractive cases, the collision can be complex and involve transient oscillating trajectories similar to those predicted by Gorshkov, Lomov & Rabinovich (1992).

Orbital motions

The orbiting pairs obtained by capture form stable and well-defined associations of walkers. These orbiting pairs can also be obtained directly. When γ_m is increased from region PDB into region W, a motionless bound state of two particles of the former region will spontaneously start rotating in the latter. This is similar to the rotating bifurcation predicted theoretically by Moskalenko *et al.* (2003) in a reaction-diffusion model where they predict that a motionless bound pair starts rotating above a well-defined threshold.

We undertook an investigation of all the possible orbits of two given identical walkers (figures 11 and 13). For drops of the same size the orbital motion is symmetrical, the particles moving around their ‘centre of mass’ (figure 11). The diameters d_n^{orb} of the possible orbits can only take a discrete set of values. The orbits being stable, after measuring one of them we disturbed it, separated the walkers and let them collide again so as to reach another orbital state. Since the oscillation frequency of the drops is half the forcing frequency, two walkers can have either the same or opposite phases. By decreasing γ_m into region B (figure 2) and then increasing it back into W it was possible to change the drops phases and thus explore the two situations with the same pair of drops.

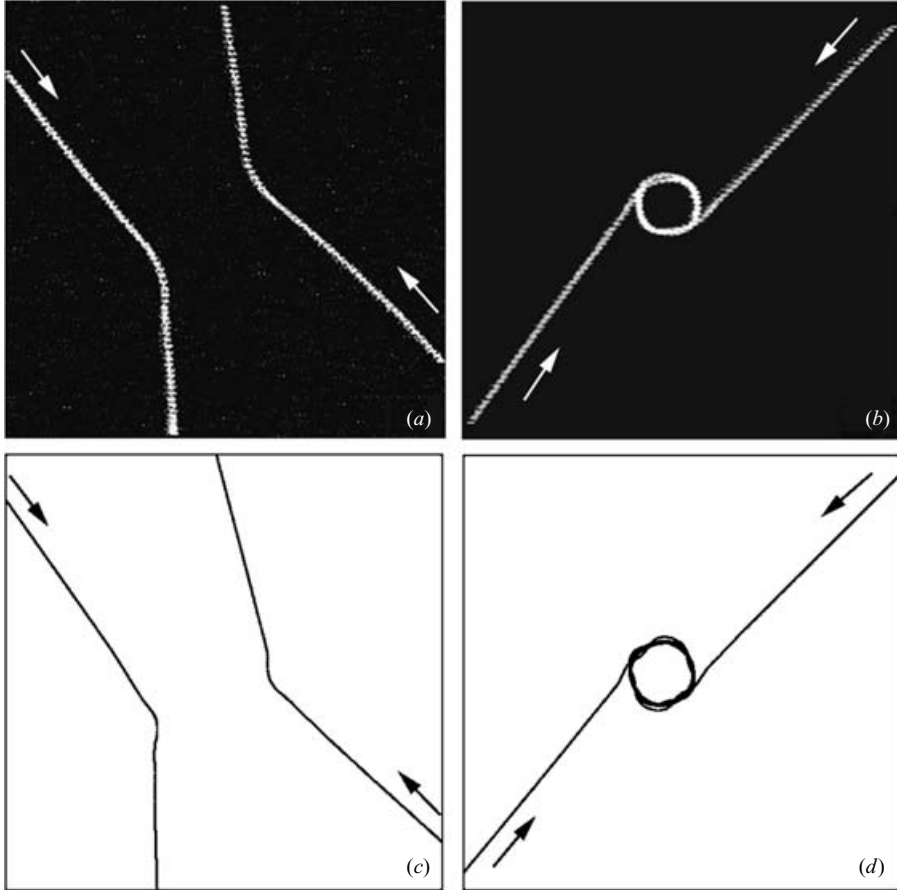


FIGURE 10. The horizontal trajectories of identical walkers in the two types of collisions they can undergo. Both are shown by a superposition of successive images obtained with drops lit from the side on a dark background ($\mu_L = 20 \times 10^{-3}$ Pa s, $f_0 = 80$ Hz). (a) Scattering of two drops by a repulsive collision (minimum distance 9 mm). (b) Mutual capture of two walkers of identical size into a circular orbit of diameter 6 mm. (c, d) Collisions obtained in the theoretical model computed using equations (7). The coefficients are estimated from the experimental characteristics and the initial conditions are chosen to recover the collisions in (a) and (b).

The measured diameters d_n^{orb} of the circular orbits of two given identical walkers form a set of discrete values which are found to be directly related to the Faraday wavelength. They can be written

$$d_n^{orb} = (n - \varepsilon_0)\lambda_F \quad (6)$$

where for drops bouncing in phase, n are the successive integers $n = 1, 2, 3, \dots$ while for drops bouncing with opposite phases the successive values of n are $1/2, 3/2, 5/2, \dots$. They are all shifted by an offset ε_0 which is the same for all orbits of these two walkers. This can be seen on figure 13(a) which is a plot of the non-dimensional diameters d_n^{orb}/λ_F of the orbits (of figure 11) as a function of their order n . At these experimental conditions ($D = 0.7$ mm, $\mu_L = 20 \times 10^{-3}$ Pa s, $f_0 = 80$ Hz, $\gamma_m/g = 3.9$) we find $\varepsilon_0 = 0.2 \pm 0.05$. For other pairs of drops having a different diameter, slightly different values of ε_0 can be found but always in the same typical range $0.15 < \varepsilon_0 < 0.25$.

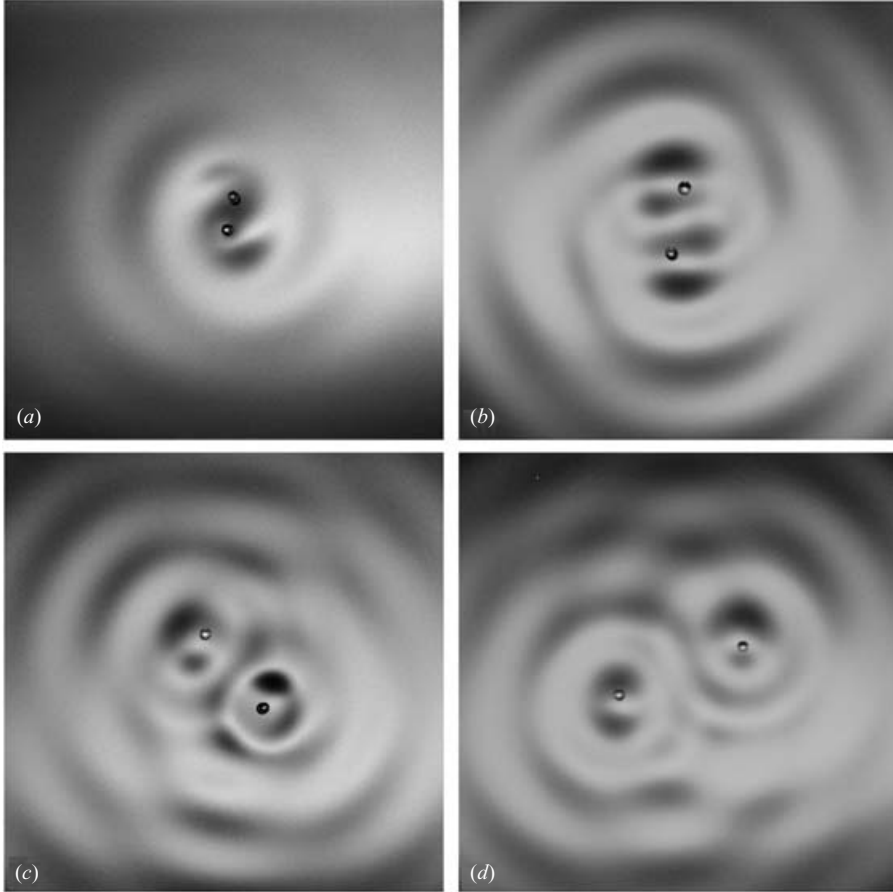


FIGURE 11. Four photographs showing the first orbital modes of identical drops bouncing on the liquid surface as seen from the top. Note that in (a) and (c) the drops bounce with opposite phases. Photograph (b) is taken exactly at the time when both drops hit the slanted surface of the waves. (a) $n = 0.5$, where $d_{0.5}^{orb} = 1.65$ mm, (b) $n = 1$, where $d_1^{orb} = 3.7$ mm, (c) $n = 1.5$, where $d_{1.5}^{orb} = 5.9$ mm, (d) $n = 2$, where $d_2^{orb} = 8.4$ mm ($D = 0.7$ mm, $\mu_L = 20 \times 10^{-3}$ Pa s, $f_0 = 80$ Hz, $\gamma_m/g = 3.9$).

Visual observation of the liquid surface (see figure 11) shows that, at the time they hit the surface, the number of antinodes of the surface wave between the two drops is $n - 1$. Because of the offset, the radius of the orbit is such that each drop, when it hits the surface, falls on the ‘inward slope’ of the wave excited by the other (see figure 11b or d and figure 15a, b). This provides at each collision the centripetal impulsion needed for orbital motion.

The periods T_n^{orb} of the motion are approximately proportional to the diameter of the orbit d_n^{orb} (figure 13b). This shows that the drops bound in an orbit have velocities V_n^{orb} slightly smaller than, but close to, the velocity V_w they had as free walkers.

Two walking drops of different diameters having thus different velocities can also form an orbiting state. The centre of rotation is then located at a distance from each drop such that, with the same angular velocity, they retain approximately the different linear velocities they had as walkers. The radius of rotation of the faster walker is thus larger than that of the slower one, so that we observe the counter-intuitive situation where the large drop rotates around a centre of rotation close to the small one.

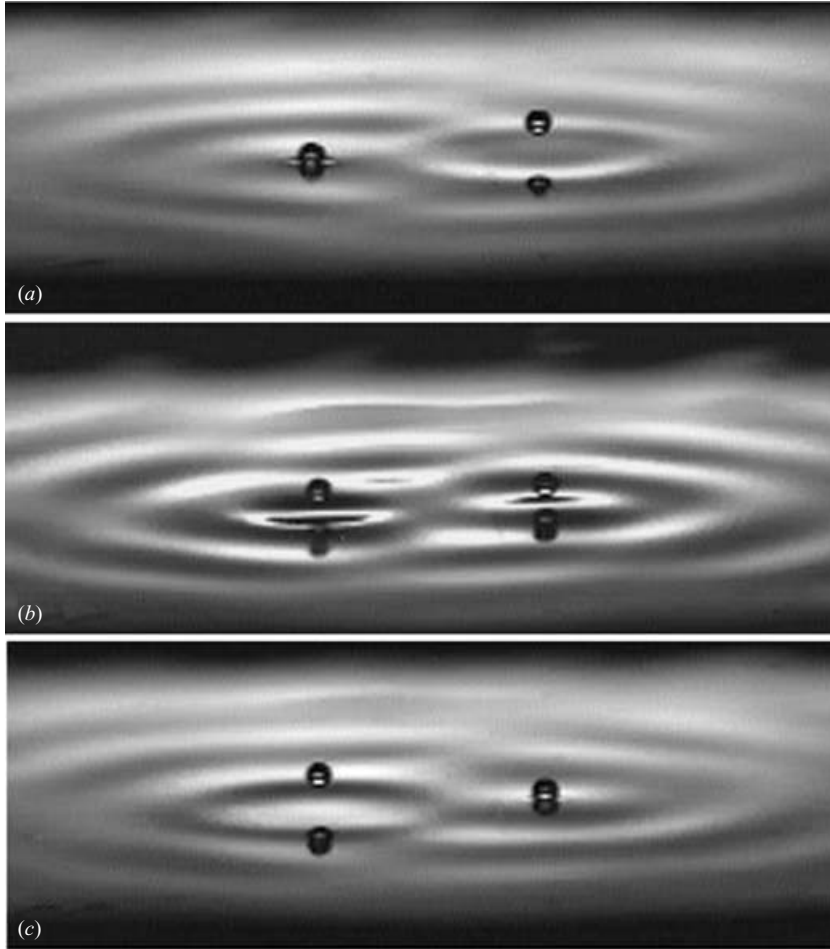


FIGURE 12. Three photographs taken with the fast camera of two orbiting drops bouncing with opposite phases as seen from the side ($D = 0.8$ mm, $d_{n=1.5}^{orb} = 5.9$ mm, $\mu_L = 20 \times 10^{-3}$ Pa s, $f_0 = 80$ Hz, $\gamma_m/g = 3.9$).

Other types of organization

Finally another mode of self-organisation of two identical drops is observed in which they form a bound pair of parallel walkers. In this situation, the two drops, at a fixed distance from each other, move with constant velocities on parallel trajectories. This mode is experimentally less frequent than orbits because the bound pair of parallel walkers is rapidly broken by collisions with the cell's walls. In a frequent variant of this type of motion, the drops move together but oscillate transversally with opposite phases.

When more drops interact, a variety of regimes are observed which are beyond the scope of this article. Let us simply note that, in the most common situation, the motion resulting from many-body interaction is chaotic. However when the number of drops is small, there can be the formation of complex organized structures. Figure 14 shows an example of the oscillating orbital motion of two large

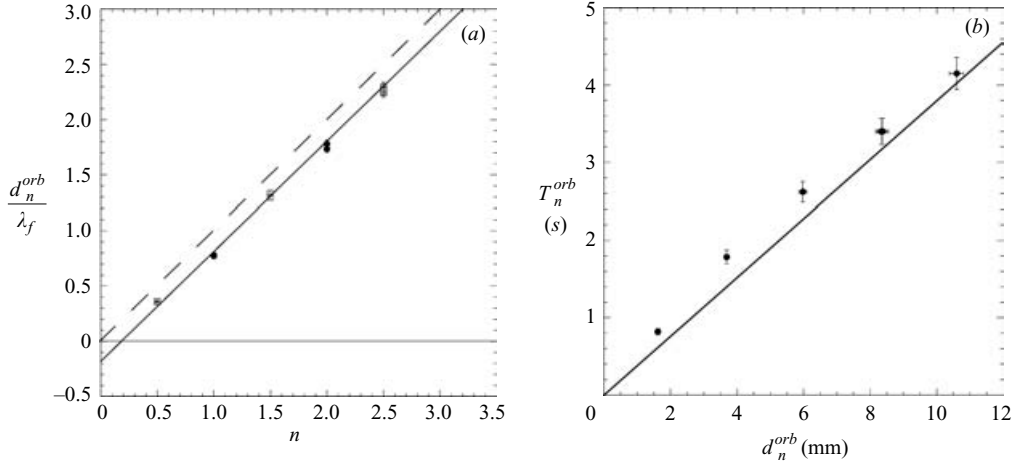


FIGURE 13. (a) The measured diameters d_n^{orb} of the orbits of two walkers as a function of their order n . The plot is of the ratio d_n^{orb}/λ_F where $\lambda_F = 4.53$ mm is the wavelength of the surface waves at the Faraday frequency. The squares correspond to two drops with the same phase, the diamonds to opposite phases. The linear extrapolation to zero of the best fit (continuous line) gives the value of ε_0 ($D = 0.7$ mm, $\mu_L = 20 \times 10^{-3}$ Pa s, $f_0 = 80$ Hz). (b) The period T_n^{orb} of the orbital motion of two given identical drops as a function of the diameter d_n^{orb} of the orbit. The line is the period that would be observed if the walkers had exactly maintained the velocity they had as free walkers.

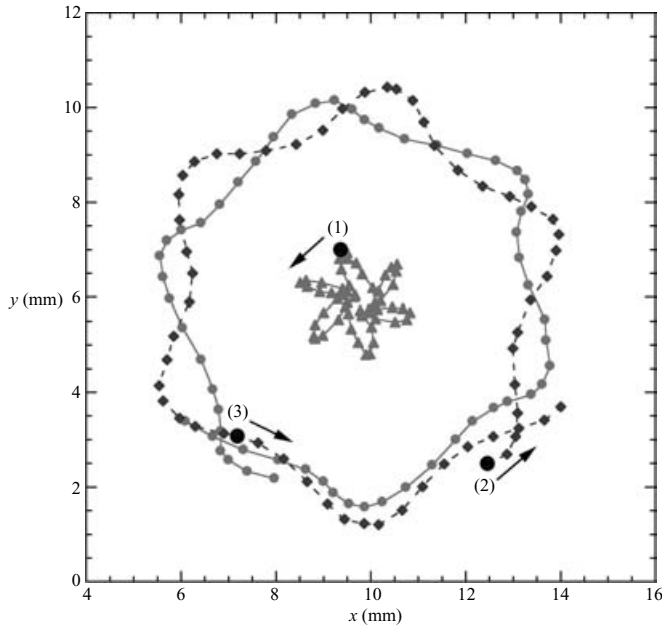


FIGURE 14. Measured trajectories of the oscillating orbiting motion of three drops of uneven sizes forming an approximately equilateral triangle ($\mu_L = 50 \times 10^{-3}$ Pa s, $f_0 = 50$ Hz, $\gamma_m/g = 4$, $D_1 = 0.5$ mm, $D_2 = 0.65$ mm, $D_3 = 0.6$ mm).

drops orbiting around a smaller one, the rotating cluster forming approximately an equilateral triangle.

4.3. A model for the interaction of walkers and their resulting self-organization

As discussed above, the motion of a walker is due to the interaction of the drop with its wave. The motion of a given drop is not only coupled to its own wave but also to any wave which disturbs the region where it bounces. When several walkers are present in a cell, the trajectory of one of them will be affected whenever the wave from another source overlaps and creates interference in the region of its bouncing. This is the source of a non-local interaction, which can be either attractive or repulsive, depending on the distance. The collisions between walkers are different from those of point-like particles because they involve the interference of two wave fields. With this type of interaction Gorshkov *et al.* (1992) predicted that it is possible to obtain chaotic scattering in the collision of two particles only. This is the origin of the oscillatory collisions we observe. We also note that the spatial extent of the wave is tunable so that the range of interaction can be chosen at will.

The horizontal motion of two interacting drops of masses m_1 and m_2 can thus be modelled with the generalization of equation (2). Two coupled vectorial equations are written (as previously, describing the motion averaged over a period T_F of the sub-harmonic vertical motion)

$$\left. \begin{aligned} m_1 \frac{d^2 \mathbf{r}_1}{dt^2} &= F_1^b \sin\left(2\pi \frac{\|\mathbf{d}\mathbf{r}_1/dt\|}{V_\phi}\right) \frac{\mathbf{d}\mathbf{r}_1/dt}{\|\mathbf{d}\mathbf{r}_1/dt\|} + \alpha F_{2 \rightarrow 1}^b \frac{(\mathbf{r}_1 - \mathbf{r}_2)}{(\mathbf{r}_1 - \mathbf{r}_2)^2} \sin(k_F \|\mathbf{r}_1 - \mathbf{r}_2\|) \\ &\quad - f_1^V \frac{d\mathbf{r}_1}{dt}, \\ m_2 \frac{d^2 \mathbf{r}_2}{dt^2} &= F_2^b \sin\left(2\pi \frac{\|\mathbf{d}\mathbf{r}_2/dt\|}{V_\phi}\right) \frac{\mathbf{d}\mathbf{r}_2/dt}{\|\mathbf{d}\mathbf{r}_2/dt\|} + \alpha F_{1 \rightarrow 2}^b \frac{(\mathbf{r}_2 - \mathbf{r}_1)}{(\mathbf{r}_2 - \mathbf{r}_1)^2} \sin(k_F \|\mathbf{r}_2 - \mathbf{r}_1\|) \\ &\quad - f_2^V \frac{d\mathbf{r}_2}{dt}. \end{aligned} \right\} \quad (7)$$

The second term on the right of each equation accounts for the interaction of each drop with the wave excited by the other. The parameters F_1^b , F_2^b , $F_{1 \rightarrow 2}^b$, $F_{2 \rightarrow 1}^b$ can be obtained as for F^b in equation (2). In (7), the parameters of the first (respectively second) equation are proportional to m_1 (respectively m_2). The interaction strength $F_{2 \rightarrow 1}^b$ ($F_{1 \rightarrow 2}^b$) is proportional to the amplitude of the wave emitted by the second (first) drop. All these parameters have the same order of magnitude. If the two drops are identical, $F_1^b = F_2^b = F_{1 \rightarrow 2}^b = F_{2 \rightarrow 1}^b = F^b$.

The parameter α (a length) takes into account two effects.

(i) The waves emitted by both drops being approximately circular, in the absence of damping their amplitudes decrease radially as $1/\|\mathbf{r}_2 - \mathbf{r}_1\|$ and a matching on a scale α_0 of the order of λ_F is necessary near the origin.

(ii) Below the Faraday threshold, the actual amplitude decrease is faster than the $1/\|\mathbf{r}_2 - \mathbf{r}_1\|$ dependence and results from a balance between the damping of the waves due to viscosity and their forcing by the imposed oscillation. The exact form of α should be $\alpha = \alpha_0 \exp(-\|\mathbf{r}_2 - \mathbf{r}_1\|/\Lambda)$, where the characteristic length Λ ($\Lambda \gg \lambda_F$) is a function of the distance to the Faraday instability threshold where it becomes infinite. In the following, for simplicity, we neglected this decrease and used $\alpha = \alpha_0 \sim \lambda_F$. Equations (7) are written for two drops bouncing in phase. The motion of drops

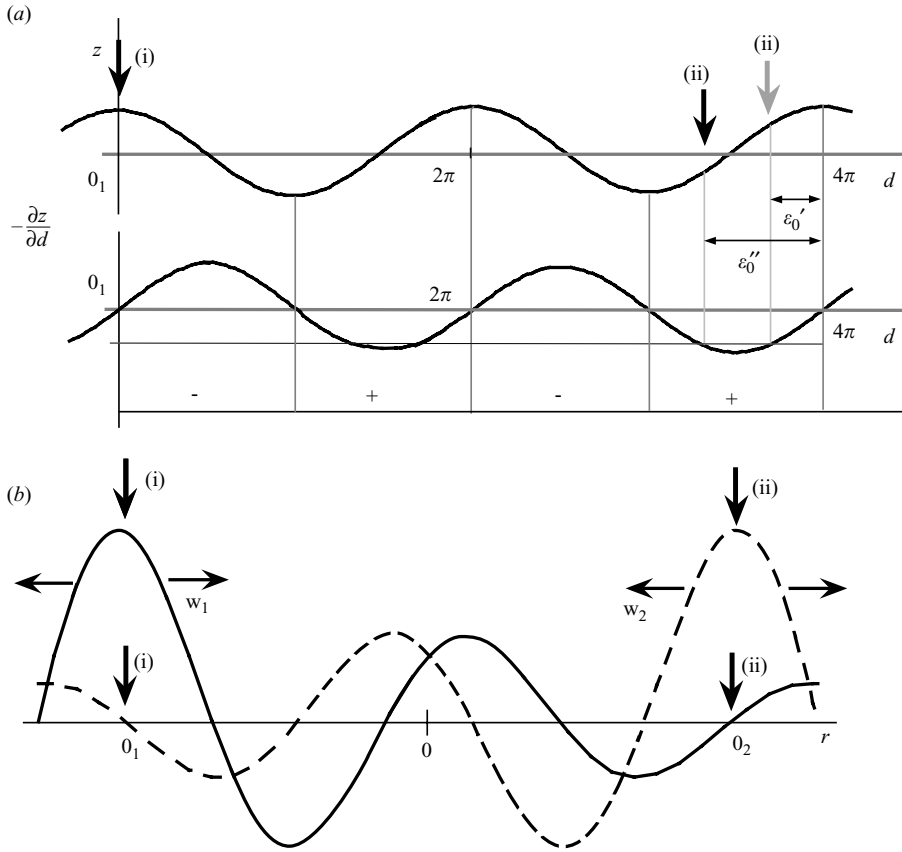


FIGURE 15. (a) Sketch of the profile and the derivative of the wave w_1 emitted by drop (i) (without its radial decrease) at the time of the collisions of the drops with the surface. Depending on the distance, the collision of (ii) with the surface will result in an attraction (regions $+$) or a repulsion (regions $-$). In the attractive region, when the two drops orbit around each other, the two possible positions of impact of the second drop (predicted by equations (7)) are shown here for mode $n=2$. The stable position is in black, the unstable one in grey. (b) Sketch of the radial cross-section of the two travelling waves w_1 and w_2 emitted by two identical orbiting drops (labelled (i) and (ii) respectively) bouncing in phase. The shape of the interface results from the superposition of these two waves. The amplitudes are drawn at the time where the two drops hit the surface. The radial damping of each wave has been included. The distance between drops corresponds to a mode $n=2$ with an offset of $\epsilon_0 = 1/4$ (fast drops).

having opposite phases can be simulated by simply changing the sign of the interaction coefficients, which corresponds to a phase shift of π .

If the proper initial conditions are chosen, the numerical integration of these ODEs yields collisional trajectories very similar to the experimental ones (figure 10c, d). On increasing the impact parameter, a succession of repulsive and attractive collisions is found, demonstrating the spatially oscillating character of the interaction (figure 15a).

We investigated quantitatively the binding of the two drops into orbital motion with quantized diameters (figure 13). Such orbits are analytical solutions of the set of equations (7). In these solutions, the velocity of each drop is constant and equal to the velocity it would have as a walker. In the radial direction, equating the force

due to the interaction term to the centrifugal effect yields (for two identical drops) a condition on the possible orbital diameters d_n^{orb} given by:

$$\sin(k_F d_n^{orb}) = -\frac{2m V_{orb}^2}{\alpha_0 F^b}. \quad (8)$$

There are two discrete sets of solutions, $d_n^{orb} = (n - \varepsilon'_0)\lambda_F$ and $d_n^{orb} = (n - \varepsilon''_0)\lambda_F$, which are both multiples of the wavelength, with two possible offset distances ε'_0 and ε''_0 defined by

$$\varepsilon'_0 = \frac{1}{2\pi} \text{Arc sin} \left(\frac{2m V_{orb}^2}{\alpha_0 F^b} \right), \quad (9)$$

$$\varepsilon''_0 = \frac{1}{2} - \frac{1}{2\pi} \text{Arc sin} \left(\frac{2m V_{orb}^2}{\alpha_0 F^b} \right) \quad (10)$$

(see the sketch in figure 15a). The numerical integration of equations (7) shows that only the second set is stable. In this set, ε''_0 is a function of the velocity of the walkers V_{orb} and ranges between 1/2 and 1/4. When the parameters corresponding to the experimental situations ($V_{orb} \sim 1 \text{ cm s}^{-1}$) are used with $\alpha = \lambda_F$, the computed orbits correspond to $\varepsilon''_0 \sim 0.45$, a value larger than found experimentally. The experimental value $\varepsilon_0 = 0.2 \pm 0.05$ is closer to the minimum value $\varepsilon''_0 = 1/4$ only obtained in the model for fast walkers when both drops impact the waves on their maximum slopes (figure 15b). This discrepancy can be ascribed to the simplifications in the theoretical model, which take into account neither the details of the collision, nor the non-instantaneous propagation of the wave. Both effects should result in a shift in the phase of the interaction waves in equation (7). This would account for the difference in the offset ε_0 between theory and experiment.

Note that if $2m V_{orb}^2 / \alpha_0 F^b$ is larger than 1, no orbital solution is possible. This is experimentally observed: very fast walkers fail to become bound into orbits because the collisions with the wave do not provide a large enough centripetal force. Numerically, when α_0 is small the attractive force is not sufficient to generate orbits.

In spite of its simplicity, this model allowed us to recover all the behaviours of two identical drops: repulsive collisions, binding into quantized orbits and binding into a parallel walk. Finally when two different masses m_1 and m_2 are set in equations (7) we recover the specific orbiting where the centre of rotation is close to the smaller drop. Overall, this model retains the essential features of the experimental system, namely the interaction of mobile real particles through the waves they excite.

5. Conclusion

Whether in the simple bouncing state or in the walking state we have obtained in these experiments phenomena characterized by the association of a particle and a wave. In the limit where no wave is emitted by the bouncing, the drops simply aggregate to form dense rafts as floating non-wetting particles would. All the other types of self-organization (solitary motion, bound states, non-compact rafts, orbits etc.) involve the non-local interaction between drops due to the waves they excite. This is a situation met in many fields of physics. In solid-state physics for example, electrons moving in a crystalline lattice emit phonons and this coupling of particles and waves leads to the formation of polarons or Cooper pairs in supra-conductors. We will limit the discussion to classical systems however. Our present results are

related to experiments which deal with self-adaptation, and to others concerned with the interaction of nonlinear wave-packets.

It was shown that adding mobile masses to bounded vibrating systems gives them additional degrees of freedom. Systems with well-defined resonances such as vibrating wires (Boudaoud, Couder & Ben Amar 1999*a*), or liquid membranes (Brazovskaia & Pieranski 1998; Boudaoud 1999*b*) thus acquire the possibility of self-adaptation. The additional mobile masses are found to exhibit a slow dynamics by which the whole system adapts to become resonant at the imposed forcing frequency. Here we also have small masses coupled to waves. Their self-organization is observed but now in a large non-resonant medium.

Comparison to the interactions and self-organization of nonlinear localized states has permitted us to clarify, by reference to them, the specificity of our system. All the classical systems in which LSs are observed have sub-critical bifurcations so that domains in a bifurcated state appear, imbedded in a basic state background. An annular region of small-amplitude waves, often called the tail of the disturbance, usually surrounds these LSs. The non-local interaction between domains is due to the interference of these waves. In our experiment the Faraday instability is super-critical and we are below its threshold. The nonlinear phenomena are thus entirely due to the bouncing of the drop, acting as a point-like disturbance. The emitted wave, which is in a damped linear regime, is, as in the case of LSs, responsible for the interaction.

Finally let us note that the dual particle/wave character of the walkers is tunable. Because of the drop's mass a walker has a real inertia but its interactions result from the waves it emits. Both characters can be adjusted: the mass of the drop can be chosen at will, while the distance to the Faraday instability threshold determines the damping distance of the wave and thus the interaction range.

We are grateful to Emmanuel Fort for enlightening discussions and to Laurent Quartier for his help in building the experimental set-up.

REFERENCES

- ARANSON, I. S., GORSHKOV, K. A., LOMOV, A. S. & RABINOVICH, M. I. 1990 Stable particle-like solutions of multidimensional nonlinear fields. *Physica D* **43**, 435–453.
- BOUDAUD, A., COUDER, Y. & BEN AMAR, M. 1999*a* A self adaptative oscillator. *Eur. Phys. J. B* **9**, 159–165.
- BOUDAUD, A., COUDER, Y. & BEN AMAR, M. 1999*b* Self-adaptation in vibrating soap films. *Phys. Rev. Lett.* **82**, 3847–3851.
- BRAZOVSKAIA, M. & PIERANSKI, P. 1998 Self-tuning behavior of vibrating smectic films. *Phys. Rev. Lett.* **80**, 5595–5598.
- CHAN, D. Y. C., HENRY, J. R. & WHITE, L. R. 1981 The interaction of colloidal particles collected at fluid interfaces *J. Colloid Interface Sci.* **79**, 410–418.
- COUDER, Y., FORT, E., GAUTIER, C. H. & BOUDAUD, A. 2005*a* From bouncing to floating drops: non-coalescence of drops on a fluid bath. *Phys. Rev. Lett.* **94**, 177801.
- COUDER, Y., PROTIÈRE, S., FORT, E. & BOUDAUD, A. 2005*b* Dynamical phenomena: Walking and orbiting droplets. *Nature* **437**, 208.
- COULLET, P., GOLDSTEIN, R. E. & GUNARATNE, G. H. 1989 Parity-breaking transitions of modulated patterns in hydrodynamic systems. *Phys. Rev. Lett.* **63**, 1954–1957.
- DEISSLER, R. J. & BRAND, H. R. 1991 Interaction of two-dimensional localized solutions near a weakly inverted bifurcation, *Phys. Rev. A* **44**, R3411–R3414.
- DESYATNIKOV, A. S. & KIVSHAR, Y. S. 2002 Rotating optical soliton clusters. *Phys. Rev. Lett.* **88**, 053901.1–4.
- EDWARDS, W. S. & FAUVE, S. 1994 patterns and quasi-patterns in the Faraday experiment. *J. Fluid Mech.* **278**, 123–148.

- FAUVE, S. & THUAL, O. 1990 Solitary waves generated by subcritical instabilities in dissipative systems. *Phys. Rev. Lett.* **64**, 282–284.
- GORSHKOV, K. A., LOMOV, A. S. & RABINOVICH, M. I. 1992 Chaotic scattering of two dimensional solitons *Nonlinearity* **5**, 1343–1353.
- LIEHR, A. W., MOSKALENKO, A. S., ASTROV, YU. A., BODE, M. & PURWINS, H.-G. 2004 Rotating bound states of dissipative solitons in systems of reaction-diffusion type. *Europhys. J. B* **37**, 199–204.
- LIUBASHEVSKI, O., ARBELL, H. & FINEBERG, J. 1996 Dissipative solitary states in driven surface waves. *Phys. Rev. Lett.* **76**, 3959–3962.
- MOSKALENKO, A. S., LIEHR, A. W. & PURWINS, H. G. 2003 Rotational bifurcation of localized dissipative structures. *Europhys. Lett.* **63**, 361–367.
- OISOPOV, V. V. 1996 Criteria of spontaneous inter-conversions of traveling and static arbitrary dimensional dissipative structures. *Physica D* **93**, 143–156.
- PIERANSKI, P. 1983 Jumping particle model. Period doubling cascade in an experimental system. *J. Phys. (Paris)* **44**, 573–578.
- PROTIÈRE, S., COUDER, Y., FORT, E. & BOUDAUD, A. 2005 The self-organization of capillary waves sources. *J. Phys.: Condens. Mat.* **17**, S3529–S3535.
- RABAUD, M., MICHALLAND, S. & COUDER, Y. 1990 Dynamical regimes of directional viscous fingering: Spatiotemporal chaos and wave propagation. *Phys. Rev. Lett.* **64** 184–187.
- SCHÄPERS, B., FELDMANN, M., ACKEMANN, T. & LANGE, W. 2000 Interaction of localized structures in an optical pattern forming system. *Phys Rev Lett.* **85**, 748–751.
- SCHENK, C. P., SCHUTZ, P., BODE, M. & PURWINS, H. G. 1998 Interaction of self organized quasiparticles in a two-dimensional reaction diffusion system: the formation of molecules. *Phys. Rev. E* **57**, 6480–6486.
- TUFILLARO, N. B. & ALBANO, A. M. 1986 Chaotic dynamics of a bouncing ball. *Am. J. Phys.* **54**, 939–944.
- UMBANHOWAR, P. B., MELO, F. & SWINNEY, H. L. 1996 Localized excitations in a vertically vibrated granular layer. *Nature* **382**, 793–796.
- VLADIMIROV, A. G., MCSLOY, J. M., SKRYABIN, D. V. & FIRTH, W. J. 2002 Two-dimensional clusters of solitary structures in driven optical cavities. *Phys. Rev. E* **65**, 046606.
- WALKER, J. 1978 Drops of liquids can be made to float on the liquid. What enables them to do so? *Sci. Am.* **238-6**, 123–129.